7B.6 **NOCTURNAL BOUNDARY LAYER HEIGHT ESTIMATE FROM DOPPLER LIDAR MEASUREMENTS**

Pichugina[1,2] Y. L., Banta[2] R. M., Kelley[3] N. D., and Brewer[2] W. A.

[1] Cooperative Institute for Research in Environmental Sciences (CIRES), Boulder, CO, U.S.A.
[2] Earth System Research Laboratory (ESRL), NOAA, Boulder, CO, U.S.A.
[3] National Wind Technology Center/National Renewable Energy Laboratory Golden, CO, U.S.A.

1. INTRODUCTION

Estimating the depth of the stable boundary layer (SBL) from measurement data has been a longstanding problem, both because of its importance for applications and because of its difficulty. Applications include the depth of dilution for air quality and emergency response, and as a scaling depth for numerical weather prediction (NWP) parameterizations of stable mixing processes. It is critical to have accurate determinations of SBL depth *h* for addressing the issue of what parameters the SBL depth depends upon.

The fundamental definition of boundary layer (BL) in general, and SBL specifically, has traditionally been turbulence based—the BL is a turbulent layer adjacent to the earth's surface. For example, Lenschow et al. (1988) and Caughey et al. (1979) used definitions based on where turbulence quantities drop to a percentage of their surface values.

Unfortunately, vertical profiles of turbulence quantities are difficult to measure, so they are not often available for determining *h*. An important question becomes, can *h* be diagnosed from mean-profile information? Such quantities as aerosol-layer depth, nocturnal temperature-inversion depth, height of the LLJ maximum, depth of a strong shear layer, and many others have all been compared, with unsatisfactory resolution to the question of which one produces the best estimate. For example, summarizing in 2000, Seibert et al. concluded that the accuracy limitation for available instrumentation at the time was about +/- 30 % for SBL depth. Tucker et al. (2009) proposed a hierarchy of estimates depending on conditions and data availability, starting with turbulence-based definitions for h, and found they could provide accurate values of h around the clock for many consecutive days, using data from Doppler lidar.

Here we use simultaneous high-resolution profiles of the mean wind speed U(z) and the streamwise velocity variance $\sigma_u^2(z)$ on 5 weakly stable nights, nights that have strong surface cooling but also strong LLJ speeds (i.e., exceeding 15 m s^{-1} during the night), to estimate SBL depths. The profiles were obtained by analyzing scan data from the high-resolution Doppler lidar (HRDL) of the National Oceanic and Atmospheric Administration's Earth System Research Laboratory (NOAA/ESRL). The variance quantity σ_u^2 has been shown to be approximately equivalent to TKE for stable conditions (Pichugina et al. 2008; Banta et al. 2006). The profiles are used to assess whether any features of the mean wind profiles U(z) can be reliably associated with the SBL depth based on $\sigma_u^2(z)$, which we designate h_σ, and if so, under what conditions? Other questions addressed include, how often can we get useful, accurate *h* information from mean profiles, and can we improve on the 30% accuracy under some conditions?

To illustrate the evolution of LLJ wind profiles observed through the night, Figure 1 shows hourly-averaged profiles of mean wind speed (top) and direction (bottom) during two strong wind nights from the Lamar experiment. These profiles were obtained from conical scans and computed by a modified velocity-azimuth display (VAD) technique, as described in Banta et al. (2002).

Wind-direction profiles typically showed modest veering with height of 10-30° over the subjet layer and 40-60° in time over ~ 10 h (Figure 1, left, bottom). For example, over a 10-h period on 15 September the direction profile rotated from ~150 to 200° close to the surface with a near-constant 10-h difference of 50° from surface up to 800 m. Wind-speed profiles that developed under such conditions in wind direction often showed clear LLJ structure with decreases in wind speed below and above the height of the LLJ maximum.

* *Corresponding author address*:
Yelena L. Pichugina, CIRES / NOAA
325 Broadway, Boulder, CO 80305
e-mail: Yelena.Pichugina@noaa.gov

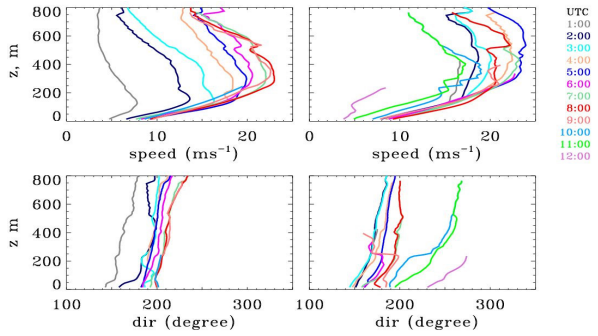

Figure 1. Hourly profiles of mean wind speed (top panels) and direction (bottom panels) during two strong wind nights from the Lamar experiment: 15 (left panels) and 9 (right panels) of September 2003. On all four panels time is indicated by different colors.

A few nights from both experiments showed strong directional variations in time and height, such as shown for the night of 9 September in the right bottom panel of Figure 1. The variations in wind direction during this night were more significant, and changes in wind direction at some heights were associated with the development of different shapes in wind-speed profiles as shown in Figure 1 (top, right).

Averaging HRDL data over shorter time intervals (10-min) produces even more variety in U(z) shapes, some of which were discussed in previous studies involving HRDL data (Banta et al. 2002, 2006). The selection of wind profiles for this study was based on certain criteria that excluded some profiles that did not show LLJ structure. In the present study, we used all 10-min profile to group them into 3 different type of shapes, as shown in Figure 2. (a) Type I: the classic LLJ shape with a distinct maximum or "nose," (b) Type II: a uniform or "flat" profile, and (c) Type III: a profile in which the shear in the subjet layer (and usually the variance profile as well) shows a layered structure.

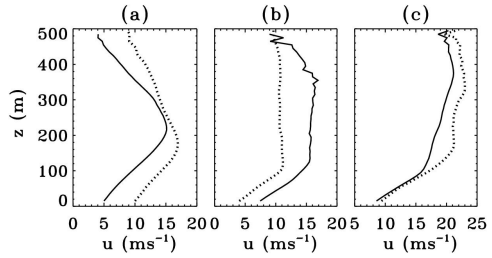

Figure 2. Two examples each of the basic types of wind-speed profile observed with HRDL measurements during the two experiments.

Not included in these types are a few profiles each night that are not classifiable for some reason, which may be instrumental, sampling (e.g., short profiles), or profiles that have a shape that does not fit any of the type definitions. LLJ evolution on any given night generally involves changes back and forth among these three types of profile shape.

Based on this classification of the wind profiles we evaluate the top of the stable boundary layer using both streamwise mean-wind and variance profiles and present results for estimates of 1) h_J, as the height of the first LLJ wind maximum above the surface; 2) top of the shear layer h_1, as the first zero-crossing or minimum of the wind shear (i.e., of the gradient or first derivative $\partial U/\partial z$ of the wind profile) below h_J (cf. Balsley et al. 2006; Tucker et al. 2009), 3) top of a sharp decrease or discontinuity in the shear at some level below h_J as the height h_2 of the first peak negative value above the surface of the curvature or second derivative $\partial^2 U/\partial z^2$. We contrast them to the height (h_σ) of the minimum in the variance profile, assuming that this is the top of the BL. Thus h_σ generally represents a level of minimum to negligible turbulence and turbulent fluxes, which isolates the rest of the atmosphere from the BL, corresponding to the turbulence-based definition of BL height.

2. DATA ACQUISITION AND ANALYSIS PROCEDURES

Profiles of the streamwise mean-wind component U(z) and the streamwise variance $\sigma_u^2(z)$ were analyzed from HRDL scan data obtained during two field projects in the Great Plains of the United States, the Cooperative Atmosphere-Surface Exchange Study campaign of October 1999 in southeastern Kansas (CASES-99), and the Lamar Low-Level Jet Project of September 2003 in southeastern Colorado. The procedures for computing mean wind and turbulence profiles from HRDL measurements of the radial or line-of-sight velocity are described in detail by Pichugina et al. (2008) and Banta et al. (2002, 2006). The profiles were calculated from the lidar scans using vertical bin sizes (i.e., vertical resolution) of 1, 5, and 10 m and over averaging time intervals of 1, 5, and 10 min (Pichugina et al. 2008). It was also shown that U(z) profiles are largely independent of the averaging parameters, although the measured variances were sensitive to these parameters. Profile data presented here are from 10-m bins and 10-min averages, but results from 5-m binning and 1-min averaging were similar as will be shown later in Figure 8.. Other than what was inherent in the sampling and averaging procedures, no further vertical smoothing or filtering was applied. In comparisons with tower-mounted sonic anemometer data (mean wind and variances) and with sodar data (for mean wind-speed profiles only), we previously found excellent agreement between mean-wind measurements, and also high correlations for the HRDL-tower turbulence intercomparisons (r = 0.8-

0.9, with several strong-wind nights having r ~0.9; see Pichugina et al. 2008), for appropriate averaging parameters. Such agreement gives us confidence in both the lidar and the sonic measurements as well as in the corresponding processing procedures.

3. RESULTS

a. Type I: Jet-nose profile

In the classic LLJ shape, U(z) profiles exhibit a distinct maximum or "nose," with U decreasing both above and below the maximum (Figure 3, red profiles, right panels).

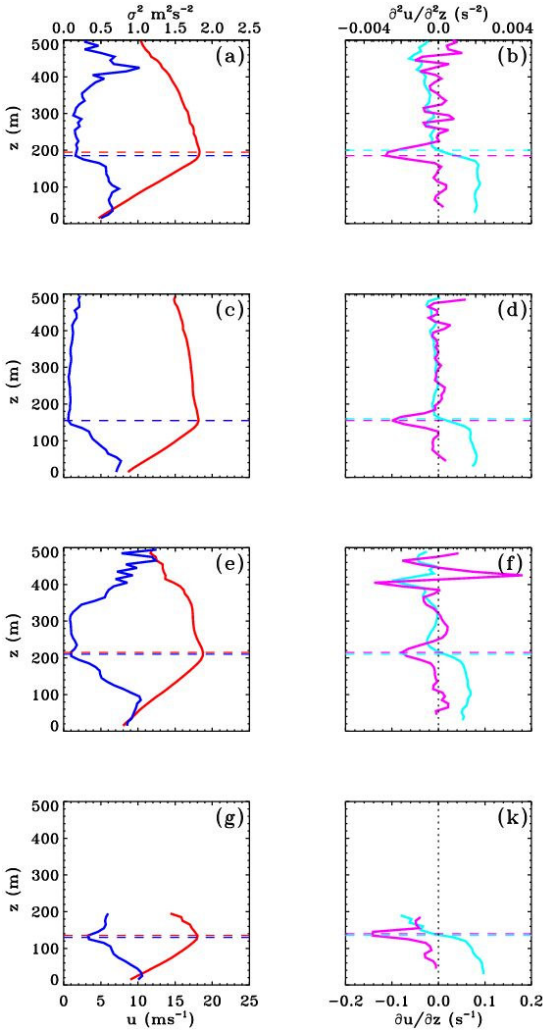

Figure 3. Example of jet-nose profiles of U(z) shown in red (left panels) and corresponding profiles of $\sigma_u^2(z)$ (blue lines, right panels), $\partial U/\partial z$ (cyan lines, left panels), and $\partial^2 U/\partial z^2$. (magenta lines, right panels). Dashed lines show h_J (red), h_σ (blue), h_1 (cyan), and h_2 (magenta).

This figure illustrates a variety of U(z) profiles even within one group. Corresponding variance, wind shear or first derivative of U(z), and second derivative of U(z) or curvature also produce a variety in shapes. The turbulence depth h_σ was determined as the first significant minimum value in the σ_u^2 profile (blue, dashed). This value, corresponding most closely to the fundamental definition of top of the SBL as marking the depth of the surface-based turbulent layer, will be taken as the reference value against which the others will be tested. Diagnostics from the mean profiles, as previously described, include h_J the height of the first LLJ maximum or nose above the surface (which was called Z_X in previous papers); h_1 the first zero crossing or minimum above the surface of the first-derivative or shear profile (cyan, right); and h_2 the first strong minimum in the curvature or second derivative of the U profile (magenta, right) above the surface, representing the first significant peak in the magnitude of the curvature, which is negative. A further constraint on h_1 and h_2 is that they must be at or below h_J. Table 1 shows that this nose profile is the most common type of profile overall and on each individual night, occurring nearly 60% of the time overall.

In a previous study a number of profiles with weak negative shear above h_J, such as Figure 3c, were included in the Type II category (BPB 2006). But because they have a distinct maximum, we have handled them differently here by including them in with the Type I sample.

Table 1. Number NN and (%) of wind-speed profiles for each study night classified by 3 types. The last column shows time of HRDL measurements during each night. Problem profiles, such as short profiles, were excluded from further analysis.

Type / Day	1	2	3	Total profs	short	Time UTC
09/05/03	42 (75)	2 (4)	10 (18)	56	2	01:09-10:50
09/06/03	27 (51)	4 (8)	18 (34)	53	4	02:20-12:00
09/09/03	22 (37)	9 (15)	22 (37)	59	6	02:00-11:50
09/15/03	34 (67)	9 (18)	5 (10)	51	3	01:00-09:40
10/25/99	40 (62)	8 (13)	7 (11)	64	9	02:30-14:50
Total	165 (58)	32 (11)	62 (22)	281	24	

The magnitude of the strong shear below the height h_J of the LLJ nose was observed to be relatively invariant within each night and from night to night, with a value of ~0.1 s^{-1} for CASES-99 (Banta et al. 2003) and somewhat less (0.08-0.09 s^{-1}) during Lamar-2003 (Banta et al. 2004). The strong subjet shear produced larger values of σ_u^2 (and TKE) near the surface (Fig. 3, left panels). Sometimes enhanced σ_u^2 was also found in the shear zone

above h_J (Figure 3 a, e), because the near-neutral lapse rates there allowed even modest shear to produce turbulence (BPB 2006). The sharp minimum in $\partial^2U/\partial z^2$, marking h_2, is clearly evident in the magenta profiles in the right panels of Figure 3. For this type of profile, h_2 corresponds closely to the turbulence-based height h_σ, as do the nose heights h_J and the shear heights h_1. Thus, for this type of U and σ_u^2 profile, all three mean-profile diagnostics work well for determining the depth of the wSBL.

b. Type II: Uniform (flat) profile

In another frequently observed profile shape, where the wind speed was relatively uniform or "flat" through a deep layer overlying the layer of strong surface-based shear (Figures 4 and 2b)..

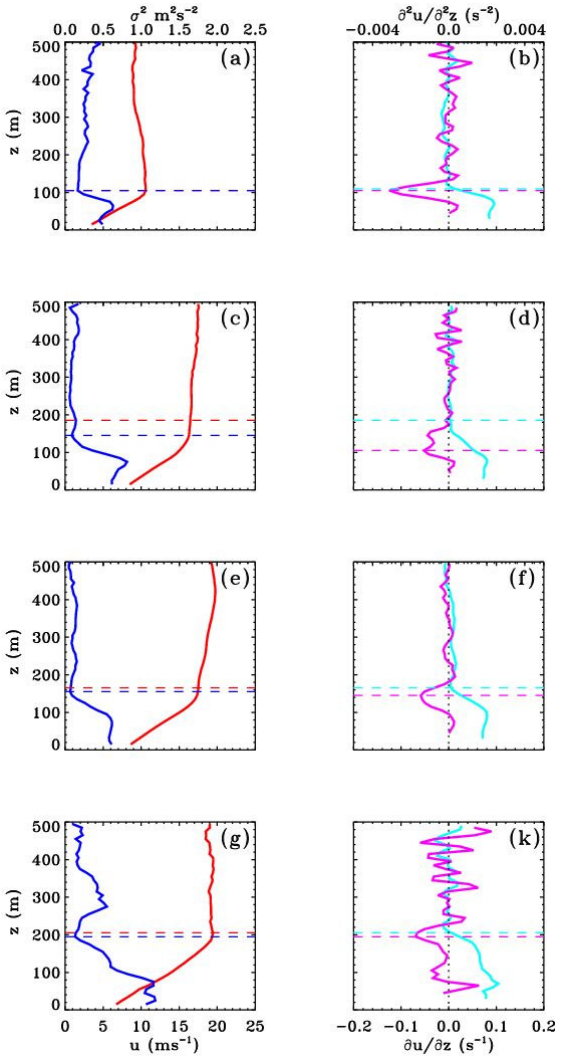

Figure 4. As in Figure 3 but for an examples of uniform (flat) profile.

Although this type of profile may not be defined as a LLJ in some studies because of the lack of a distinct nose, for present purposes it qualifies as a LLJ because it represents an acceleration of the wind over the late-afternoon well-mixed flow, and therefore the winds are stronger in this accelerated layer than at some heights above this layer (e.g., see solid profile in Figure 2b). Overall this type of profile was observed more than 10% of the time, but it was observed in 18% of the profiles on 15 September 2003 (Table 1).

It is evident for this type of profile that the large values of σ_u^2 were confined to the strong shear layer adjacent to the surface (Figure 4, right panels).

Turbulence in the weak-shear layer aloft was mostly negligible (cf. Figure 4c, e), although occasional transient bursts in this layer could be seen (e.g., at ~300 m in Figure 4g). Thus, as with the Type I profiles, h_σ clearly corresponds to the first zero (or minimum) in shear h_1, and this altitude also corresponds to the peak minimum in the U-profile curvature h_2. However, the uniform-velocity layer aloft was not well mixed as a result of negligible turbulence in this layer, so weak maxima in U(z) could appear at any level within this layer (e.g., $\boldsymbol{h_1}$ ~ 430 m in Figure 4e). Thus, h_J was not always a reliable indicator of h_σ for this category.

c. Type III: Layered profile

Type I and II profiles were characterized by linear or gently curved U profiles (nearly constant speed shear), and small directional shear below the LLJ height for the weakly stable, strong-LLJ conditions of this study. A number of profiles (22% overall as listed in Table 1) had a discontinuity or step in the shear at one or more levels below the LLJ nose, as shown in Figure 5. The shear above the step was smaller than the shear below (Figure 5, right panels, cyan line), and σ_u^2 values were also larger below the steps (Figure 5, left panels, blue profiles). In these cases it was often difficult to specify the top of the SBL h_σ at all, because σ_u^2 values in layers aloft (above the surface-based layer of stronger turbulence) were often non-negligible, indicating the continuous existence of turbulence in the vertical from the surface up through the top of the shear layers aloft (Figure 5, d,f,k). A substance released at the surface would be diffused rapidly in the vertical through the first layer, then more slowly through the second and subsequent layers aloft. The issue of which level represents the SBL top thus depends on the strength of the turbulence in the upper layers and the time requirement (if any) for vertical diffusion to qualify as part of the SBL. For example, many authors have required interaction with the surface over periods of an hour or less for a vertical level to be considered part of the SBL (e.g., Stull 1988; Beyrich et al. 1997; Seibert et al. 2000).

Type III structure was often found during transient periods, for example, as the height of the LLJ nose moved upward (or downward) in response to changes in large-scale forcing, as illustrated in BPB 2006 (Fig. 6 of that paper). However on some nights, this structure was observed to persist for an hour (as in Fig 8a) or several hours (as during the nights of September 6 and 9, Table 1), and thus did not appear to be a transient structure during these periods.

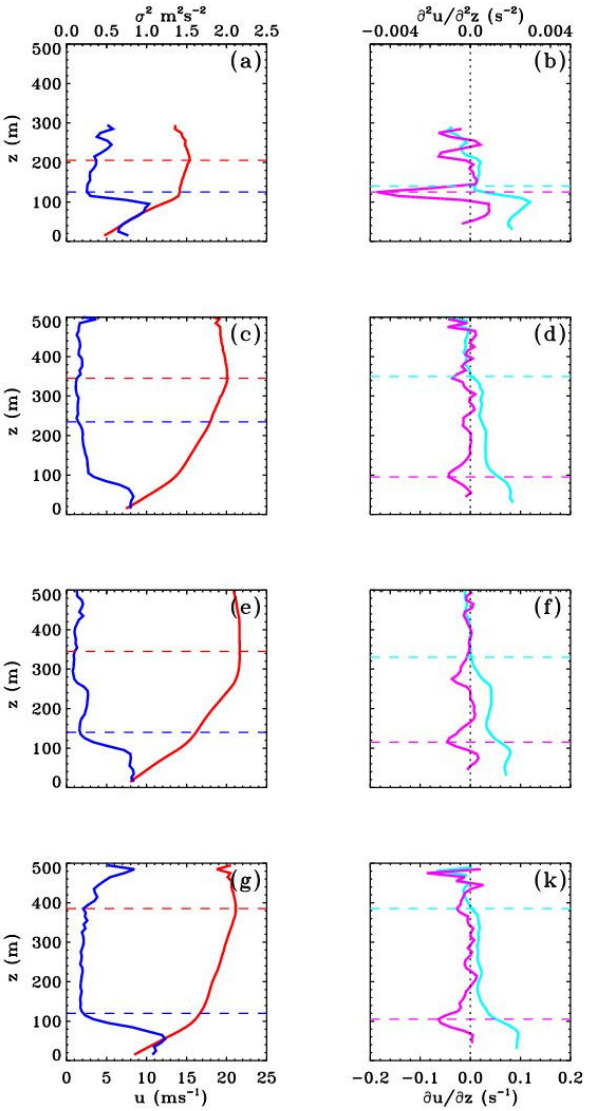

Figure 5. As in Figure 3 but for an examples of layered profile.

d. Regression analysis

Each of the three mean-profile diagnostics (h_J, h_1, and h_2) was compared with the reference SBL depth h_σ using regression analyses. The results are presented in scatter diagrams in Figure 6 for two nights: (a) October 25, 1999 and (b) September 15, 2003.

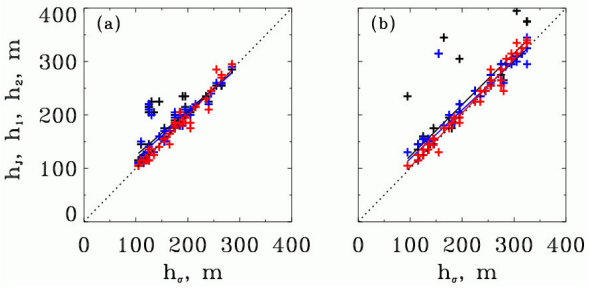

Figure 6. Scatter plots of h_J (black), h_1 (blue), and h_2 (red) vs. h_σ for the night from each experiment. Solid lines in both panels (also in tree colors) are linear regression fit for these scatters.

These plots show very good correlations between h_2 and h_σ for both nights. On the other hand, the heights h_J and h_1 were significantly higher than h_σ in several cases, mostly when profiles exhibited layered structure. Such profiles were observed from 0600 to 0700 UTC during the night of 25 October 1999 and at 0210, 0630, 0700, and 0910-0940 UTC during the night of 15 September 2003 (also see Figure 8). Correlation coefficients for all scatter plots in Figure 6 along with equations of the least-squares fit are shown in Table 2.

Table 2. Correlation coefficient, slope, and bias for the relations between h_σ and h_J, h_1, h_2 Statistics are shown for two strong wind nights: 25 October from Cases-99 experiment and 15 September form Lamar experiment.

Day	$h_\sigma = A_J + B_J h_J$			$h_\sigma = A_1 + B_1 h_1$			$h_\sigma = A_2 + B_1 h_2$		
	R_J	A_J	B_J	R_1	A_1	B_1	R_2	A_2	B_2
10/25/99	0.81	39.9	0.84	0.86	29.6	0.87	0.98	-1.77	1.0
09/15/03	0.84	26.4	0.96	0.93	26.2	0.92	0.99	0.99	1.01

The usefulness of these diagnostics depends on how accurately they estimate $\boldsymbol{h_\sigma}$. As a measure of this accuracy, histograms of the magnitude of the difference between $\boldsymbol{h_2}$ and $\boldsymbol{h_\sigma}$, normalized by $\boldsymbol{h_\sigma}$, are given in Figure 7 for one night from each experiment. Most of the estimates lie within 10%, and the standard deviation of the difference is 5%. Thus, for these nights, the curvature estimate of the SBL depth $\boldsymbol{h_2}$ was accurate to within 5% of the depth. Evaluations of the other depth diagnostics and assessments for the other nights are in progress.

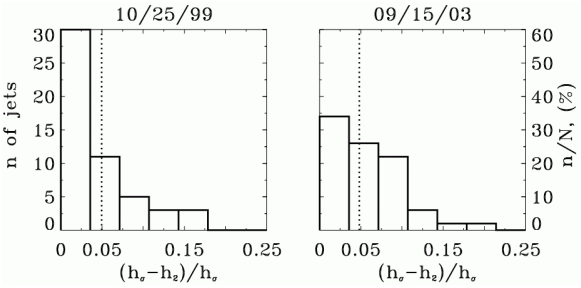

Figure 7. Histograms of the normalized absolute value of the difference between h_σ, and h_2 computed for two nights: 25 October 1999 and 15 September 2003. Dotted lines on both plots indicate standard deviations of this error, which equal approximately 5% in each case.

e. Time-height cross sections

To illustrate the evolution of *h* and its relationship to turbulence in the SBL, Figure 8 shows time-height cross sections of $\sigma_u^2(z)$ for the nights shown in Figures 6,7, based on 1-min profiles of these quantities. Superimposed on these cross sections are the 10-min values of each of the SBL depth estimates, h_σ, h_J, h_1, and h_2. For these cases it is evident that overall, the *h*'s tend to cluster at the top of a surface-based turbulent layer (the SBL) at a level of minimum turbulence in the vertical.

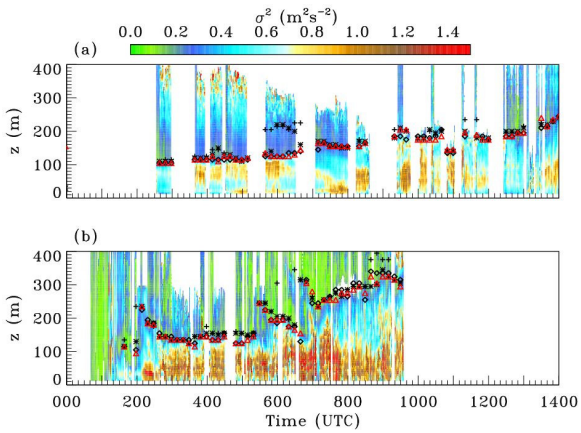

Figure 8. Time-height cross sections of horizontal wind variance for the nights of (a) October 25, 1999 and (b) September 15, 2003. The height of the LLJ wind maximum (h_J) is shown in both panels by black plus signs: black asterisks and diamonds show h_1, and h_2. Red triangles show the height of the minimum in the variance profile (h_σ.). Abscissa: time in UTC, ordinate: height (m, AGL)

4. CONCLUSIONS

The high temporal and spatial resolution of the HRDL data allowed investigation of wind-speed and turbulence conditions in great detail within the stable boundary layer. Quantities of interest that were monitored using Doppler lidar included mean LLJ properties (speed, height, direction) and characteristics of the turbulence below the jet, including estimates of the SBL depth. The detailed profiles of the streamwise mean-wind component U(z), which was approximately equal to the mean wind speed, and streamwise variance $\sigma_u^2(z)$, which was approximately equal to TKE, showed that it was possible to obtain good estimates of the SBL depth $\boldsymbol{h_\sigma}$ from the mean profile data ~70% of the time overall, using the shear-derived estimate h_1 or the curvature-derived estimate h_2, and nearly 60% of the time using h_J. Given that the data were discretized at 10-m vertical resolution, the estimates $\boldsymbol{h_1}$ and $\boldsymbol{h_2}$ were mostly coincident with $\boldsymbol{h_\sigma}$ for Types I and II profiles, occasionally being off by one increment. Problem profile shapes accounting for the other 30% were mostly those having a layered structure to the shear. Over all of the profile shapes, $\boldsymbol{h_2}$ performed best, with root-mean-square departures of ~5% from $\boldsymbol{h_\sigma}$ for the entire sample of Types I-III.

Thus, under stable conditions, when wind profiles show clear LLJ structure, all heights $\boldsymbol{h_J}$, $\boldsymbol{h_\sigma}$, $\boldsymbol{h_1}$, and $\boldsymbol{h_2}$ tended to be equal or very close. For the periods of the late-afternoon (00 - ~03 UTC) and early-morning (09-12 UTC) transitions, or when profiles of the mean wind show several maxima or a discontinuity below $\boldsymbol{h_J}$, the heights often disagreed. In these instances the height based on the curvature of the mean-wind profile $\boldsymbol{h_2}$ was generally better correlated with the height of the turbulence layer $\boldsymbol{h_\sigma}$.

ACKNOWLEDGMENTS: Field data acquisition and portions of the analysis for this research were funded by the National Renewable Energy Research Laboratory (NREL) of the U.S. Department of Energy (DOE) under Interagency Agreement DOE-AI36-03GO13094. Portions of the analysis were also supported by the U.S. Army Research Office (Dr. Walter Bach) of the Army Research Laboratory under Proposal No. 43711-EV, and analysis and manuscript preparation were also supported by the NOAA Air Quality and Health of the Atmosphere Programs. The NREL work was supported by the U.S. Department of Energy under contract No. DE-AC36-99GO10337. We thank our colleagues Rob Newsom, Volker Wulfmeyer, Scott Sandberg, Janet Machol, Brandi McCarty, Joanne George, Raul Alvarez, Andreas Muschinski, Jennifer Keane, Ann Weickmann, Ron Richter, R.M. Hardesty, J. Otten, W. Eberhard, and Lisa Darby from ESRL, and the following from NREL: Mari Shirazi, Dave Jager, S. Wilde and J. Adams. We also wish to acknowledge

the Emick family, on whose ranch the Lamar project took place.

The height of the minimum value of the second derivative of the mean wind speed profile was found to be in good agreement with the height of the minimum or steepest decrease in the variance profile, which corresponds to the top of the SBL.

REFERENCES

Balsley, B.B., R.G. Frehlich, M.L. Jensen, and Y. Meillier, 2006: High-resolution in-situ profiling through the stable boundary layer: Examination of the SBL top in terms of minimum shear, maximum stratification, and turbulence decrease. *J. Atmos. Sci.*, **63**, 1291-1307.

Banta, R.M., R.K. Newsom, J.K. Lundquist, Y.L. Pichugina, R.L. Coulter, and L. Mahrt 2002: Nocturnal low-level jet characteristics over Kansas during CASES-99. *Bound.-Layer Meteor.*, **105**, 221-252.

_____, Y.L. Pichugina, and R.K. Newsom, 2003: Relationship between low-level jet properties and turbulence kinetic energy in the nocturnal stable boundary layer. *J. Atmos. Sci.*, **60**, 2549-2555.

_____, _____, and W.A. Brewer (2006), Turbulent velocity-variance profiles in the stable boundary layer generated by a nocturnal low-level jet. *J. Atmos. Sci.*, **63**, 2700-2719. *[denoted **BPB 2006**]*

_____, L. Mahrt, D. Vickers, J. Sun, B. Balsley, Y. Pichugina, and E. Williams, 2007: The very stable boundary layer on nights with weak low-level jets, *J. Atmos. Sci.*, **64**, 3068-3090.

_____, 2008: Stable-boundary-layer regimes from the perspective of the low-level jet. *Acta Geophysica*, **56**, 58-87.

Beyrich, F., 1997: Mixing height estimation from sodar data – A critical discussion. *Atmos. Environ.*, **31**, 3941-3953.

Blumen, W., R.M. Banta, S.P. Burns, D.C. Fritts, R. Newsom, G.S. Poulos, and J. Sun, 2001: Turbulence statistics of a Kelvin-Helmholtz billow event observed in the nighttime boundary layer during the CASES-99 field program. *Dynamics of Atmos. and Oceans*, **34**, 189-204.

Caughey, S.J., J.C. Wyngaard, and J. C. Kaimal, 1979: Turbulence in the evolving stable boundary layer. *J. Atmos. Sci.*, **36**, 1041-1052.

Grund, C. J., R. M. Banta, J. L. George, J. N. Howell, M. J. Post, R. A. Richter, A. M. Weickmann, 2001: High-resolution Doppler lidar for boundary layer and cloud research. *J. Atmos. Oceanic Technol.*, **18**, 376-393.

Kelley, N, B.J. Jonkman, G.N. Scott, Y.L. Pichugina, 2007: Comparing Pulsed Doppler Lidar with Sodar and Direct Measurements for Wind Assessment. *NREL/CP-500-41792, Golden, CO: National Renewable Energy Laboratory.*

Lenschow, D.H., X. S. Li, C.-J. Zhu, and B.B. Stankov, 1988: The stably stratified boundary layer over the Great Plains. I. Mean and turbulent structure. *Bound.-Layer Meteor.*, **42**, 95-121.

Lundquist, J. and Mirocha J., 2007: Interaction of nocturnal low-level jets with urban geometries as seen in Joint Urban 2003 Data. *J. Appl. Met. and Clim.*, **47**, 44-58

Mahrt, L., 1999: Stratified atmospheric boundary layers. *Bound.-Layer Meteor.* **90**, 375-396.

_____, and D. Vickers, 2002: Contrasting vertical structures of nocturnal boundary layers. *Bound.-Layer Meteor.*, **105**, 351-363.

_____, and _____, 2006, Extremely weak mixing in stable conditions, *Bound.-Layer Meteor.*, **119**, 19-39.

Mahrt, L., R.C. Heald, D.H. Lenschow, B.B. Stankov, and I. Troen, 1979: An observational study of the structure of the nocturnal boundary layer, *Bound.-Layer Meteor.*, **17**, 247- 264.

Mahrt, L., J. Sun, W. Blumen, T. Delaney, and S. Oncley, 1998: Nocturnal boundary layer regimes, *Bound.-Layer Meteor.*, **88**, 255-278.

Pichugina, Y.L., R.M. Banta, N.D. Kelley, S.P. Sandberg, J.L. Machol, and W.A. Brewer (2004), Nocturnal low-level jet characteristics over southeastern Colorado, *16th Symposium on Boundary Layers and Turbulence, Portland ME*, Paper 4.11, 6 pp. (preprints).

_____, _____, W.A. Brewer, N.D. Kelley, R.K. Newsom, and S.C. Tucker, 2008: Evaluation of Doppler-lidar-based horizontal-velocity and turbulence profiles to averaging procedures, *J. Atmos. Ocean. Technol.*, **24,** (in press).

_____, _____, N. D. Kelley, 2007: Analysis of the southern Colorado Low-Level jet by high resolution Doppler Lidar data. Comparison to the Great Plains LLJ climatologies. *3d Symposium on Lidar Atmospheric Applications*, San Antonio, TX, (preprints)..

Poulos, G.S., W. Blumen, D.C. Fritts, J.K. Lundquist , J. Sun, S. Burns, C. Nappo, R.M. Banta, R.K. Newsom, J. Cuxart, E. Terradellas, B. Balsley, M.

Jensen, 2002: CASES-99: A comprehensive investigation of the stable nocturnal boundary layer., *Bull. Amer. Meteor. Soc.*, **83**, 555-581.

Seibert, P., F. Beyrich, S.-E. Gryning, S. Joffre, A. Rasmussen, and P. Tercier, 2000: Review and intercomparison of operational methods for the determination of the mixing height. *Atmos. Environ.*, **34**, 1001-1027.

Stull, R. B.: 1988, *An Introduction to Boundary-Layer Meteorology.* Kluwer Acad. Publ., Dordrecht, 666 pp.

Tucker, S.C., W.A. Brewer, R.M. Banta, C.J. Senff, S.P. Sandberg, D. Law, A.M. Weickmann, and R. M. Hardesty, 2009: Doppler lidar estimation of mixing height using turbulence, shear, and aerosol profiles. *J. Atmos. Oceanic Technol.*, **25**, submitted.

Vogelezang, D.H.P., and A.A.M. Holtslag, 1996: Evaluation and model impacts of alternative boundary-layer height formulations. *Bound.-Layer Meteor.*, **81**, 245-269.